Chapter 6

The planar tendon-driven parallel manipulator

6.1 Introduction

Tendon-driven parallel manipulators represent a relatively recent technology, characterized by the use of cables in place of the linear actuators generally used in parallel manipulators. The use of these manipulators as overhead cranes for materials handling (Dagalakis *et al.* [123], Bostelman *et al.* [124], Verhoeven *et al.* [125]) and worker-access (Bostelman *et al.* [126]) in the heavy, and large-scale manufacturing industries appears to be a promising application of this technology. On a smaller scale another possible application of tendon driven manipulators is in pick-and-place applications. Verhoeven *et al.* [125] also mention applications as fast moving micromanipulators.

Three separate, but inter-related topics are examined in this chapter, and methodologies for addressing these topics are proposed. The first topic addressed is the determination of cable forces for overconstrained tendon-driven manipulators. It is necessary to solve this problem in order to address the

second topic, namely the development of a methodology for workspace determination of tendon-driven manipulators. The final topic examined is the dimensional synthesis of tendon-driven manipulators for a large dextrous workspace.

As far as the current state-of-the-art relating to these topics is concerned, Verhoeven and Hiller [127] present a method for determining the cable tension distribution in overconstrained tendon-based parallel manipulators. This method is limited though to the homogenous case, where no external forces are applied to the manipulator end-effector. Lafourcade *et al.* [128] determine cable tensions based on the minimum norm solution. In terms of workspace calculation, Verhoeven and Hiller [129] have proposed a method for determining planar tendon-driven manipulator workspaces considering external forces, but not torques applied to the moving platform. Other authors, for example, Fattah and Agrawal [130] have used a discretization approach to determining and optimizing manipulator workspaces.

In the next section, the tendon-driven parallel manipulators considered in this chapter are presented and the kinematic and static analyses performed. Thereafter methods for determining cable forces are developed and described. Two methodologies for determining workspaces of tendon-driven parallel manipulators are developed and applied to 3- and 4-cable planar tendon-driven parallel manipulators. Finally dimensional synthesis of these manipulators for maximal dextrous workspaces is performed.

6.2 The tendon-driven parallel manipulator

As shown schematically in Figure 6.1, the tendon-driven parallel manipulator (TDPM) considered here consists of a moving platform connected to a fixed frame by means of n cables, with associated displacement vectors $\boldsymbol{\ell}^i = [\ell_x^i, \ell_y^i]^\top$, $i = 1, \ldots, n$. The lengths of the cables, denoted l_i, $i = 1, \ldots, n$

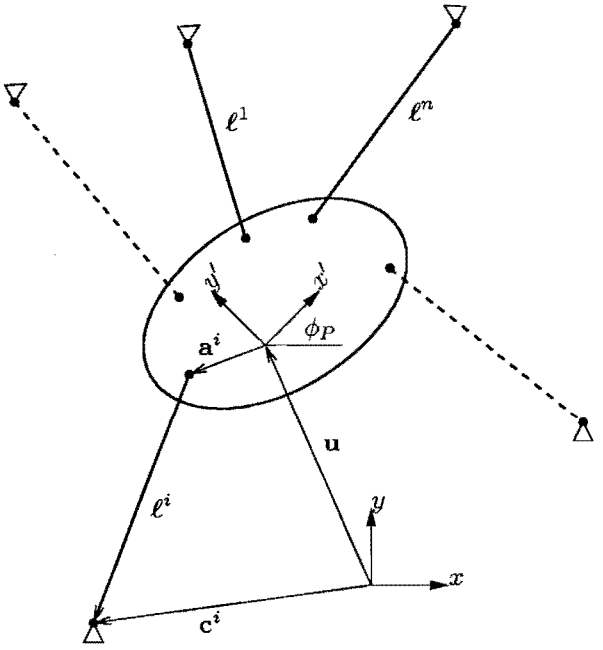

Figure 6.1: Planar tendon-driven manipulator definitions

where $l_i = \ell^i = \|\ell^i\|$, can be varied by winches attached to the fixed frame. A coordinate frame $x' - y'$ is attached to the moving platform. The position of the origin of the platform coordinate frame is $\mathbf{u} = [u_1, u_2]^\top = [x_P, y_P]^\top$, and the platform frame is inclined at an angle ϕ_P to the global $x - y$ coordinate frame. The cables are attached to the fixed frame at $\mathbf{c}^i$, $i = 1, \ldots, n$ and to the moving platform at points $\bar{\mathbf{a}}^i, i = 1, \ldots, n$, defined relative to the platform coordinate frame $x' - y'$. These vectors may of course be transformed to the global coordinate frame by means of a transformation matrix $\mathbf{T}(\phi_P)$ such that the global attachment vectors $\mathbf{a}^i$ are given by $\mathbf{a}^i = \mathbf{T}(\phi_P)\bar{\mathbf{a}}^i$. The forces in each of the cables are described by vectors $\mathbf{f}^{Ci} = [f_x^{Ci}, f_y^{Ci}]^\top$, $i = 1, 2, \ldots, n$. The corresponding magnitudes of the tensions in these cables are denoted $t_i, i = 1, 2, \ldots, n$ where $t_i = f^{Ci} = \|\mathbf{f}^{Ci}\|$. External forces and torques acting on the platform are $\mathbf{f}^P = [f_x^P, f_y^P, \tau^P]^\top$.

The specific planar parallel tendon-driven manipulator used to illustrate the methodologies proposed here is shown in Figure 6.2. It is assumed that the

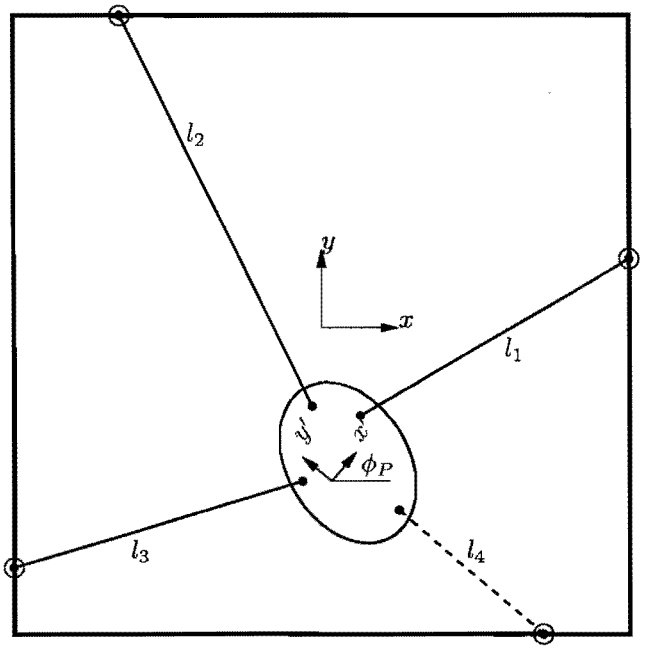

Figure 6.2: The planar tendon-driven manipulator

	3-cable	4-cable
$\bar{\mathbf{a}}^1$	$\frac{1}{\sqrt{2}}[0.1, 0.1]^\top$	$\frac{1}{\sqrt{2}}[0.1, 0.1]^\top$
$\bar{\mathbf{a}}^2$	$\frac{1}{\sqrt{2}}[-0.1, 0.1]^\top$	$\frac{1}{\sqrt{2}}[-0.1, 0.1]^\top$
$\bar{\mathbf{a}}^3$	$[0.0, -0.1]^\top$	$[-0.1, -0.1]^\top$
$\bar{\mathbf{a}}^4$	-	$[0.1, -0.1]^\top$

Table 6.1: TDPM moving platform cable attachment points

motors are positioned somewhere on a square frame of dimensions 2×2 in arbitrary units. The global origin $x - y$ is positioned at the center of the frame. Two different configurations, a 3-cable and a 4-cable manipulator will be considered. For each of these configurations, the cable attachment points on the moving platform platform are given in Table 6.1, and the exact motor attachment points on the frame in Table 6.2. The workspace of the manipulator is dependent on the load applied to the platform. In this chapter, three different load cases, denoted L1-L3, and given in arbitrary units in Table 6.3, will be considered.

	3-cable	4-cable
$\mathbf{c}^1$	$[1,1]^\mathsf{T}$	$[1,0.5]^\mathsf{T}$
$\mathbf{c}^2$	$[-1,1]^\mathsf{T}$	$[-1,0.5]^\mathsf{T}$
$\mathbf{c}^3$	$[0,-1]^\mathsf{T}$	$[-1,-0.5]^\mathsf{T}$
$\mathbf{c}^4$	-	$[1,-0.5]^\mathsf{T}$

Table 6.2: Geometrical parameters for the 3 and 4-cable TDPM

	f_x^P	f_y^P	τ^P
L1	0	-10	0
L2	5	-10	0
L3	5	-10	1

Table 6.3: Load conditions L1-L3

6.2.1 Kinematic analysis

Consider the n kinematic constraint equations, expressed in generalized coordinates $\mathbf{q} = [\mathbf{u}, \mathbf{v}, w]^\mathsf{T}$, relating the platform position $\mathbf{u} = [x_P, y_P]^\mathsf{T}$, the orientation $w = \phi_P$, and the input cable lengths $\mathbf{v} = [l_1, l_2, \ldots, l_n]^\mathsf{T}$:

$$\mathbf{\Phi}(\mathbf{q}) = \mathbf{\Phi}(\mathbf{u}, \mathbf{v}, w) = \mathbf{0} \tag{6.1}$$

From Figure 6.1, it can be seen that the following relationships hold:

$$\boldsymbol{\ell}^i = \mathbf{c}^i - \mathbf{a}^i(\phi_P) - \mathbf{u}, \; i = 1, 2, \ldots, n \tag{6.2}$$

The transformation $\mathbf{a}^i(\phi_P) = \mathbf{T}(\phi_P)\bar{\mathbf{a}}^i$ of $\bar{\mathbf{a}}^i$ from the local to the global coordinate system, by means of the matrix $\mathbf{T}(\phi_P)$, is given by

$$\begin{bmatrix} a_x^i \\ a_y^i \end{bmatrix} = \begin{bmatrix} \cos\phi_P & -\sin\phi_P \\ \sin\phi_P & \cos\phi_P \end{bmatrix} \begin{bmatrix} \bar{a}_x^i \\ \bar{a}_y^i \end{bmatrix} \tag{6.3}$$

for $i = 1, 2, \ldots, n$. The corresponding input cable lengths $l_i = \|\boldsymbol{\ell}^i\|$ may be written as:

$$\begin{aligned} l_i &= \left[(\ell_x^i)^2 + (\ell_y^i)^2\right]^{\frac{1}{2}} \\ &= \left[(c_x^i - a_x^i(\phi_P) - x_P)^2 + (c_y^i - a_y^i(\phi_P) - y_P)^2\right]^{\frac{1}{2}} \end{aligned} \tag{6.4}$$

Writing (6.4) in the standard form (6.1) yields

$$\begin{aligned}\boldsymbol{\Phi}(\mathbf{q}) &= \boldsymbol{\Phi}(\mathbf{u}, \mathbf{v}, w) \\ &= \begin{bmatrix} v_1 - \left[(c_x^1 - a_x^1(w) - u_1)^2 + (c_y^1 - a_y^1(w) - u_2)^2\right]^{\frac{1}{2}} \\ v_2 - \left[(c_x^2 - a_x^2(w) - u_1)^2 + (c_y^2 - a_y^2(w) - u_2)^2\right]^{\frac{1}{2}} \\ \vdots \\ v_n - \left[(c_x^n - a_x^n(w) - u_1)^2 + (c_y^n - a_y^n(w) - u_2)^2\right]^{\frac{1}{2}} \end{bmatrix} \\ &= \mathbf{0}\end{aligned} \tag{6.5}$$

where a subscript x, y or z denotes the x, y or z component of a vector. Substituting (6.3) into (6.5) and differentiating yields

$$\boldsymbol{\Phi}_{\mathbf{q}}\dot{\mathbf{q}} = \begin{bmatrix} \frac{\ell_x^1}{l_1} & \frac{\ell_y^1}{l_1} & \frac{(\mathbf{a}^1 \times \boldsymbol{\ell}^1)_z}{l_1} & 1 & 0 & \cdots & 0 \\ \frac{\ell_x^2}{l_2} & \frac{\ell_y^2}{l_2} & \frac{(\mathbf{a}^2 \times \boldsymbol{\ell}^2)_z}{l_2} & 0 & 1 & \cdots & 0 \\ \vdots & \vdots & \vdots & \vdots & \vdots & \ddots & \vdots \\ \frac{\ell_x^n}{l_n} & \frac{\ell_y^n}{l_n} & \frac{(\mathbf{a}^n \times \boldsymbol{\ell}^n)_z}{l_n} & 0 & 0 & \cdots & 1 \end{bmatrix} \begin{bmatrix} \dot{u}_1 \\ \dot{u}_2 \\ \dot{w} \\ \dot{v}_1 \\ \dot{v}_2 \\ \vdots \\ \dot{v}_n \end{bmatrix} = \mathbf{0} \tag{6.6}$$

This can alternatively be written as

$$\begin{bmatrix} \dot{v}_1 \\ \dot{v}_2 \\ \vdots \\ \dot{v}_n \end{bmatrix} = - \begin{bmatrix} \frac{\ell_x^1}{l_1} & \frac{\ell_y^1}{l_1} & \frac{(\mathbf{a}^1 \times \boldsymbol{\ell}^1)_z}{l_1} \\ \frac{\ell_x^2}{l_2} & \frac{\ell_y^2}{l_2} & \frac{(\mathbf{a}^2 \times \boldsymbol{\ell}^2)_z}{l_2} \\ \vdots & \vdots & \vdots \\ \frac{\ell_x^n}{l_n} & \frac{\ell_y^n}{l_n} & \frac{(\mathbf{a}^n \times \boldsymbol{\ell}^n)_z}{l_n} \end{bmatrix} \begin{bmatrix} \dot{u}_1 \\ \dot{u}_2 \\ \dot{w} \end{bmatrix} \text{ or } \dot{\mathbf{v}} = -\mathbf{J}\left[\dot{\mathbf{u}}^\top, \dot{w}\right]^\top \tag{6.7}$$

where $\mathbf{J}$ is the Jacobian of the kinematic constraint equations with respect to the output $\mathbf{u}$ and intermediate w variables.

6.2.2 Static analysis

Force equilibrium implies that for any configuration, specified by $\mathbf{u}$ and w, the following equations must hold:

$$\sum_{i=1}^{n} \mathbf{f}^{Ci} + [f_x^P, f_y^P]^\top = \mathbf{0} \text{ and } \sum_{i=1}^{n} \mathbf{a}^i \times \mathbf{f}^{Ci} + \tau^P = 0 \tag{6.8}$$

Noting that the tensions $\mathbf{f}^{Ci}$ act parallel to their corresponding cable vectors $\boldsymbol{\ell}^i$, it follows that

$$\mathbf{f}^{Ci} = \frac{\boldsymbol{\ell}^i}{l_i} t_i \tag{6.9}$$

Equations (6.8) can thus be rewritten as

$$\sum_{i=1}^{n} \frac{\boldsymbol{\ell}^i}{l_i} t_i + [f_x^P, f_y^P]^\top = \mathbf{0} \text{ and } \sum_{i=1}^{n} \mathbf{a}^i \times \frac{\boldsymbol{\ell}^i}{l_i} t_i + \tau^P = 0 \tag{6.10}$$

where $l_i = \|\boldsymbol{\ell}^i\|$. Writing (6.10) in matrix form gives

$$\begin{bmatrix} f_x^P \\ f_y^P \\ \tau^P \end{bmatrix} = - \left[\begin{array}{ccc|c} \frac{\ell_x^1}{l_1} & \frac{\ell_x^2}{l_2} & \frac{\ell_x^3}{l_3} & \cdots \; \frac{\ell_x^n}{l_n} \\ \frac{\ell_y^1}{l_1} & \frac{\ell_y^2}{l_2} & \frac{\ell_y^3}{l_3} & \cdots \; \frac{\ell_y^n}{l_n} \\ \frac{(\mathbf{a}^1 \times \boldsymbol{\ell}^1)_z}{l_1} & \frac{(\mathbf{a}^2 \times \boldsymbol{\ell}^2)_z}{l_2} & \frac{(\mathbf{a}^3 \times \boldsymbol{\ell}^3)_z}{l_3} & \cdots \; \frac{(\mathbf{a}^n \times \boldsymbol{\ell}^n)_z}{l_n} \end{array}\right] \begin{bmatrix} t_1 \\ t_2 \\ t_3 \\ \hline \vdots \\ t_n \end{bmatrix} \tag{6.11}$$

$$\text{or } \mathbf{f}^P = -\mathbf{S}\mathbf{t}$$

where $\mathbf{S}$ is called the *structure matrix* of the manipulator (Verhoeven *et al.* [125]). It is interesting to note that $\mathbf{S} = \mathbf{J}^\top$, where $\mathbf{J}$ is the Jacobian defined by equation (6.7).

6.3 Calculation of the cable tensions

6.3.1 Minimum norm approach

It is evident for the planar case, as pointed out by Verhoeven and Hiller [127] and Fattah and Agrawal [130], that system (6.11) is overconstrained

and thus has many solutions if $n > 3$. For $n = 3$ there are 3 equations and 3 unknowns, and thus if the equations are linearly independent, there will be a unique solution simply given by

$$\mathbf{t} = -\mathbf{S}^{-1}\mathbf{f}^P \tag{6.12}$$

For $n > 3$ there are many solutions, assuming $\mathbf{S}\mathbf{S}^\top$ is invertible. The general solution to (6.11) in this case is of the form

$$\mathbf{t} = \mathbf{t}^{\text{mn}} + \mathbf{t}^{\text{nul}} \tag{6.13}$$

where $\mathbf{t}^{\text{mn}}$ is the minimum norm solution of (6.11) and $\mathbf{t}^{\text{nul}}$ is a vector belonging to the nullspace $\mathcal{N}(\mathbf{S})$ of $\mathbf{S}$. The minimum norm solution $\mathbf{t}^{\text{mn}}$ is determined by means of the Moore-Penrose inverse, defined as $\mathbf{S}^+ = \mathbf{S}^\top(\mathbf{S}\mathbf{S}^\top)^{-1}$, and is given by (Fattah and Agrawal [130])

$$\mathbf{t}^{\text{mn}} = -\mathbf{S}^+\mathbf{f}^P = -\mathbf{S}^\top(\mathbf{S}\mathbf{S}^\top)^{-1}\mathbf{f}^P \tag{6.14}$$

Fattah and Agrawal [130] take $\mathbf{t}^{\text{nul}} = \mathbf{0}$ and thus the solution to (6.11) is simply given by setting $\mathbf{t} = \mathbf{t}^{\text{mn}}$ where $\mathbf{t}^{\text{mn}}$ is given by (6.14). As will be illustrated in the next section this approach may result in some feasible points being excluded from the workspace. The minimum norm solution does however have the advantage that it is not computationally demanding, and may thus have some use when performing rough workspace calculations. Lafourcade *et al.* [128] present a simple iterative method whereby $\mathbf{t}^{\text{nul}}$ is gradually increased until feasible cable tensions are determined.

6.3.2 Constrained ℓ_2-norm approach

A new methodology for determining the cable tensions for any specified $\mathbf{u}$ and w is now proposed. Using the partitioning indicated in system (6.11) to define

$$\mathbf{f}^P = -\left[\mathbf{A}\middle|\mathbf{B}\right]\left[\mathbf{t}^{A\top}\middle|\mathbf{t}^{B\top}\right]^\top \tag{6.15}$$

where $\mathbf{A}$ is 3×3 and $\mathbf{B}$ is $3 \times (n-3)$, system (6.11) can be rewritten as:

$$\mathbf{t}^A(\mathbf{t}^B) = -\mathbf{A}^{-1}\mathbf{f}^P - \mathbf{A}^{-1}\mathbf{B}\mathbf{t}^B \tag{6.16}$$

which gives the values of the dependent tensions $\mathbf{t}^A \in \Re^3$ as a function of the independent tensions $\mathbf{t}^B \in \Re^{n-3}$. For a given position $\mathbf{u} = [x_P, y_P]^\mathsf{T}$ and orientation $w = \phi_P$ of the platform, and for identical prescribed lower and upper bounds, $t^{\min}$ and $t^{\max}$ on the tension magnitudes t_i, $i = 1, 2, \ldots, n$, the cable tensions $\mathbf{t}$ may now be determined by solving the following numerical optimization problem[1]:

$$\begin{aligned} &\min_{\mathbf{t}^B} \|\mathbf{t}\|_2^2 \\ &\text{such that } t^{\min} \leq t_i^A(\mathbf{t}^B) \leq t^{\max},\ i = 1, 2, 3 \\ &\text{and } t^{\min} \leq t_j^B \leq t^{\max},\ j = 1, 2, \ldots, (n-3) \end{aligned} \tag{6.17}$$

where $\mathbf{t} = [t_1, t_2, \ldots, t_n]^\mathsf{T} = [\mathbf{t}^{A\mathsf{T}}, \mathbf{t}^{B\mathsf{T}}]^\mathsf{T} = [t_1^A, t_2^A, t_3^A, t_1^B, \ldots, t_{n-3}^B]^\mathsf{T}$. This optimization problem is solved using the LfopC numerical optimization algorithm of Snyman [103] (see Appendix B). Of course, on removal of the inequality constraints, it can be shown that optimization problem (6.17) reduces to equation (6.14) (see Appendix E). The advantage of the methodology proposed here is that either the minimum, or maximum possible cable tensions, in the case where a maximization is performed instead in (6.17), can be determined. The respective solutions correspond to a tendon driven system with minimal energy consumption, or one with maximal stiffness.

Figure 6.3 illustrates the significant difference between the minimum norm (with $\mathbf{t}^{\text{nul}} = \mathbf{0}$) and constrained ℓ_2-norm approach approaches for determining the cable tensions. The illustrative manipulator design analyzed here has frame attachment points $\mathbf{c}^1 = [1, 0.15]^\mathsf{T}$, $\mathbf{c}^2 = [-1, 0.15]^\mathsf{T}$, $\mathbf{c}^3 = [-1, -0.15]^\mathsf{T}$ and $\mathbf{c}^4 = [1, -0.15]^\mathsf{T}$ and platform attachment points as given in Table 6.1. The constant orientation workspaces for $\phi_P = 0$, $\phi_P = 0.2$ and $\phi_P = 0.4$ are given. Minimum and maximum allowable tensions were 5 and 100 respectively. The workspaces indicated by a solid line were calculated using

[1] $\|\cdot\|_2$ denotes the ℓ_2-norm of its argument.

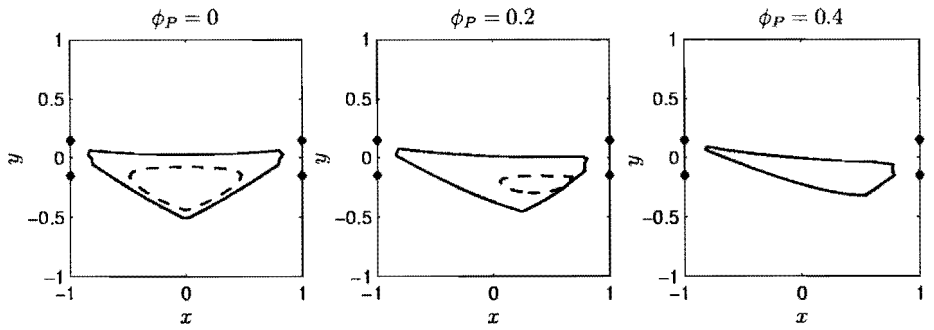

Figure 6.3: Comparison of workspaces obtained with cable forces calculated using the minimum norm (dashed line) and constrained ℓ_2-norm (solid line) approaches.

the constrained ℓ_2-norm approach, and those indicated by a dashed line were calculated using the unconstrained minimum norm approach for determining the cable tensions. Workspaces were determined using the chord method (see Section 6.4.3). It is evident that using the unconstrained minimum norm solution here results in an extreme underestimation of the feasible workspace of the manipulator.

6.3.3 Constrained ℓ_1-norm approach

The constrained ℓ_2-norm approach for determining cable tensions outlined above is limited by the computational effort required by the numerical optimization algorithm. When determining manipulator workspaces, for example, the cable tensions will have to be determined many times. It is thus desirable to have a more efficient method for determining the feasible cable tensions. The constrained ℓ_1-norm approach follows from the constrained ℓ_2-norm approach outlined above, but is posed as a linear programming problem, allowing for a more efficient solution of the cable tensions. For a fixed position and orientation of the moving platform, the constraints on the three dependent cable tensions $\mathbf{t}^A$ are used to calculate the feasible region for the

independent cable tensions $\mathbf{t}^B \in \Re^{n-3}$. For each dependent cable, minimum and maximum tension limits dictate that the following inequalities hold:

$$\begin{aligned} t^{\min} - t_i^A(\mathbf{t}^B) \leq 0,\ i = 1,2,3 \\ \text{and } t_i^A(\mathbf{t}^B) - t^{\max} \leq 0,\ i = 1,2,3 \end{aligned} \tag{6.18}$$

Defining $\mathbf{M} = -\mathbf{A}^{-1}\mathbf{f}^P$ and $\mathbf{N} = -\mathbf{A}^{-1}\mathbf{B}$, substituting (6.16) into (6.18), and including the inequalities limiting the tensions of the independent cables $\mathbf{t}^B$ the feasible region in the independent cable tension space $\mathbf{t}^B \in \Re^{n-3}$ is bounded by the inequality constraints of the following optimization problem[2]:

$$\begin{aligned} \min_{\mathbf{t}_B} \|\mathbf{t}\|_1 = \min_{\mathbf{t}_B} \left(\sum_{p=1}^{n} t_p^A(\mathbf{t}^B) + \sum_{q=1}^{n-3} t_q^B \right) \\ \text{such that} \\ \sum_{j=1}^{n-3} N_{ij} t_j^B \geq t^{\min} - M_i,\ i = 1,2,3; \\ \sum_{j=1}^{n-3} N_{ij} t_j^B \leq t^{\max} - M_i,\ i = 1,2,3 \\ \text{and } t^{\min} \leq t_k^B \leq t^{\max},\ k = 1,2,\ldots,(n-3) \end{aligned} \tag{6.19}$$

The minimum or maximum (where a maximization is performed instead) allowable cable tensions may be determined by solving optimization problem (6.19). For $n \geq 5$ this can be done efficiently using linear programming methods. For the case where $n = 4$, inequalities (6.19) reduce to

$$\begin{aligned} N_i t^B \geq (t^{\min} - M_i),\ i = 1,2,3 \\ N_i t^B \leq (t^{\max} - M_i),\ i = 1,2,3 \\ 0 \leq t^{\min} \leq t^B \leq t^{\max} \end{aligned} \tag{6.20}$$

The existence of a feasible solution, and the minimum $t^{B\min}$ and maximum $t^{B\max}$ allowable independent cable tensions may in this case be easily and efficiently determined analytically by examining the extreme values of t^B

[2] $\|\cdot\|_1$ denotes the ℓ_1-norm of its argument.

defined by (6.20). The exact algorithm achieving this is stated in Algorithm 6.1.

Algorithm 6.1 Tension limit algorithm

for $i = 1:3$
  if $N_i > 0$
    $t_i^{\text{low}} = (t^{\min} - M_i)/N_i$
    $t_i^{\text{high}} = (t^{\max} - M_i)/N_i$
  else
    $t_i^{\text{low}} = (t^{\max} - M_i)/N_i$
    $t_i^{\text{high}} = (t^{\min} - M_i)/N_i$
  end if
end for
$t_4^{\text{low}} = t^{\min}$
$t_4^{\text{high}} = t^{\max}$
$t^{B\min} = \max_i(t_i^{\text{low}}),\ i = 1,\ldots,4$
$t^{B\max} = \min_i(t_i^{\text{high}}),\ i = 1,\ldots,4$

If $t^{B\min} > t^{B\max}$, then no feasible solution exists for the cable tensions. Of course, once t^B is known, the dependent cable tensions $\mathbf{t}^A$ may be calculated using (6.16). Note that since the minimum ℓ_1-norm solution may correspond to *either* $t^{B\min}$ or $t^{B\max}$, it is necessary to evaluate and compare both possibilities in order to determine the correct minimum norm. The same is true when determining the maximum ℓ_1-norm. In terms of control of such a manipulator, the cable tensions $\mathbf{t}$ corresponding to either $t^{B\min}$ or $t^{B\max}$, or indeed any intermediate values, may be used since these are all feasible solutions for the cable tensions.

6.4 Constant orientation workspace determination

6.4.1 Workspace definition

Unlike regular parallel manipulators, where the workspace is dependent on the input joint limits and the geometrical realization of the manipulator, the workspace for tendon-driven manipulators is primarily determined by the allowable forces in the cables (Verhoeven *et al.* [125]). In particular, the tension in each of the cables should lie between a pretension and maximum tension:

$$t^{\min} \leq t_i \leq t^{\max}, \ i = 1, 2, \ldots, n \tag{6.21}$$

Here it is also required that each cable has a minimum allowable length $l^{\min}$:

$$l_i \geq l^{\min}, \ i = 1, 2, \ldots, n \tag{6.22}$$

The constant orientation workspace $W^C[w^{\text{fix}}]$ (as defined in Section 1.3.1) of the tendon-driven parallel manipulator for a fixed platform orientation $w^{\text{fix}} = \phi_P^{\text{fix}}$ can now be defined as

$$\begin{aligned} W^C[w^{\text{fix}}] = \{ & \mathbf{u} \in \Re^2 : \mathbf{\Phi}(\mathbf{u}, \mathbf{v}, w^{\text{fix}}) = \mathbf{0}, \\ & t^{\min} \leq t_i \leq t^{\max} \text{ and } l_i \geq l^{\min}, \ i = 1, 2, \ldots, n \} \end{aligned} \tag{6.23}$$

Where the cable tensions $\mathbf{t}$ are calculated using either the minimum norm, constrained ℓ_2-norm, or constrained ℓ_1-norm approach proposed in the previous section, and the cable lengths $\mathbf{v}$ are calculated using (6.4). Other conditions such as platform stiffness and proximity to singularities can also be easily included in the workspace definition by the addition of further inequality constraints. In this chapter, for the the 3-cable manipulator, a lower limit is placed on the determinant of the kinematic Jacobian, to ensure that the manipulator does not approach a singular position:

$$\det(\mathbf{J}) \geq D^{\min} \tag{6.24}$$

Limit	Value
$t^{\min}$	5
$t^{\max}$	100
$l^{\min}$	0.1
$D^{\min}$	10^{-3}

Table 6.4: Numerical values of limits used in calculating TDPM workspaces

The values of the various maximum and minimum limits required in inequalities (6.21), (6.22) and (6.24), as used for all numerical examples in this chapter, are given in Table 6.4.

6.4.2 Discretization method

As mentioned in Section 1.3.2, one method commonly used by researchers for determining parallel manipulator workspaces is the discretization method. For a given fixed orientation ϕ^{fix} of the moving platform, this method simply involves discretizing the output space $\mathbf{u} \in \Re^2$ of the planar TDPM at a given resolution, and then testing each of the resulting mesh points $\mathbf{u}^{ij}$ for compliance with the inequalities (6.21) and (6.22), as well as (6.24) if applicable. If none of these inequalities are violated then the point lies within the manipulator workspace. If any of the constraints are violated, then the point does not lie within the workspace. The basic discretization method used is stated in Algorithm 6.2.

This discretization method has been applied to workspace determination of various manipulator designs, using the constrained ℓ_2-norm method, embodied in (6.17) for determining the cable tensions in the 4-cable case.

Algorithm 6.2 Discretization algorithm

1. Select the required workspace resolution, m, specifying the number of points to be inserted between the maximum and minimum possible limits of the workspace determined in the next step.

2. Determine extreme limits of the region to be discretized by determining $x^{\min} = \min(c_x^i)$, $x^{\max} = \max(c_x^i)$, $y^{\min} = \min(c_y^i)$, and $y^{\max} = \max(c_y^i)$ for $i = 1, 2, \ldots, n$ in each case.

3. Discretize the output space of the manipulator by determining $(m+1)^2$ points $\mathbf{u}^{ij} = [x^{\min} + \frac{i}{m}(x^{\max} - x^{\min}), y^{\min} + \frac{j}{m}(y^{\max} - y^{\min})]^\top$ for $i = 0, 1, 2, \ldots, m$ and $j = 0, 1, 2, \ldots, m$.

4. Test each $\mathbf{u}^{ij}$ for compliance with inequalities (6.21) and (6.22) (and (6.24) for the 3-cable case). If all inequalities are satisfied, record $\mathbf{u}^{ij}$ as a valid point.

3-cable manipulator

Constant orientation workspaces for the 3-cable manipulator described in Section 6.2, and for values of $\bar{\mathbf{a}}^i$ and $\mathbf{c}^i$ as defined in Tables 6.1 and 6.2 respectively, were calculated using the discretization method. Figure 6.4 shows the constant orientation workspaces obtained for[3] $\phi_P = 0$, $\phi_P = 0.05$ and $\phi_P = 0.1$ in the columns, and for load cases L1, L2 and L3 (given in Table 6.3) in the rows. For these cases, using $m = 50$, the average time for workspace calculation was 0.03s, using a FORTRAN code on a 1.6 GHz Pentium 4 computer. Of course, as m is increased, the time required for computation increases proportionally to m^2.

It is interesting to note, for this manipulator design, that the manipulator workspace is highly dependent on the both the load on the moving platform,

[3]All angles in this chapter are expressed in radians.

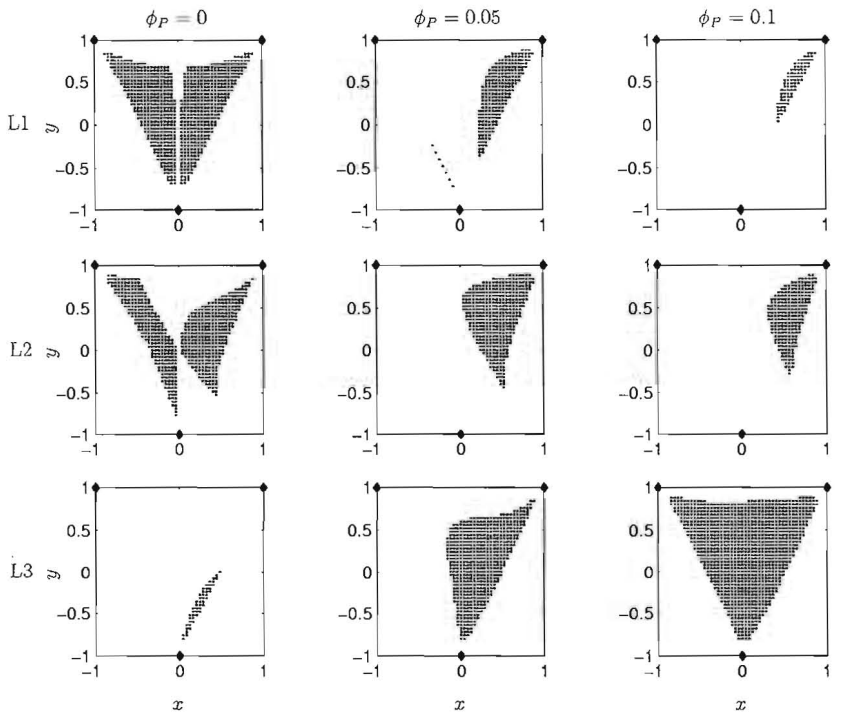

Figure 6.4: Workspaces of the 3-cable TDPM determined using the discretization method

as well as the orientation of the platform. Note that even small changes in the platform orientation result in extreme changes in the workspace. Also of interest is the presence of a singularity at $x = 0$ for the cases where $\phi_P = 0$ which effectively divides the workspace into two usable regions. The workspace boundaries in the vicinity of this singularity are dictated by the limit $D^{\min}$ on the determinant of the Jacobian, implemented by means of inequality (6.24).

4-cable manipulator

Figure 6.5 shows some constant orientation workspaces of the 4-cable manipulator presented in Section 6.2, and defined in Tables 6.1 and 6.2. These

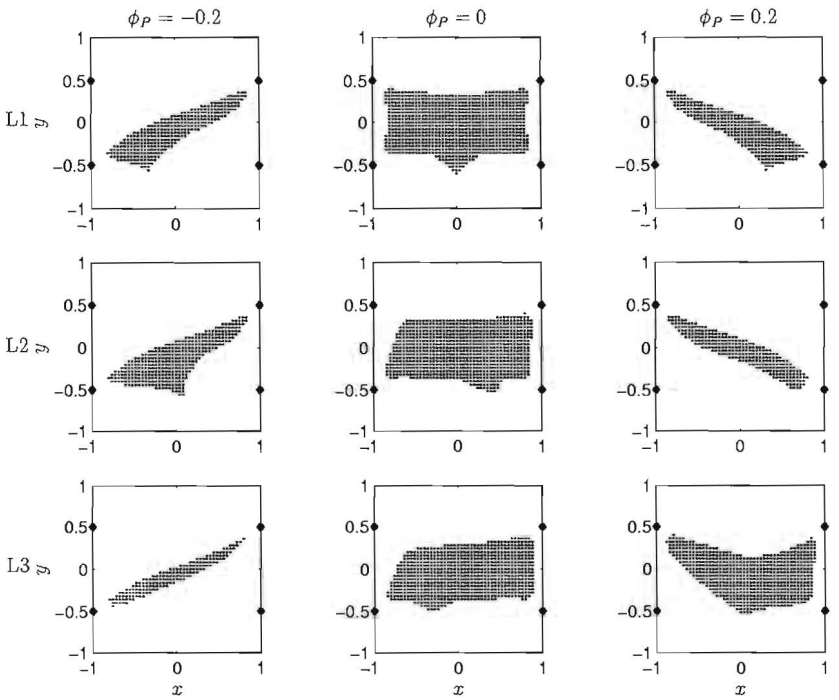

Figure 6.5: Workspaces of the 4-cable TDPM determined using the discretization method

workspaces were calculated using the discretization algorithm with $m = 50$, and the constrained ℓ_2-norm method embodied in (6.17) for determining the cable tensions. The average time for workspace computation was 29.3s, using FORTRAN on a 1.6 GHz Pentium 4 computer. It is immediately evident that the necessity of using a more complicated approach for determining the cable tensions for the 4-cable manipulator dramatically increases the time required to compute the manipulator workspace. Times required to compute workspaces using the constrained ℓ_1-norm approach for determining cable tensions are comparable to the 3-cable case.

Of interest is the fact that for the particular design presented here, the manipulator has a greater workspace than for the 3-cable manipulator. It also appears that the size of the workspace is less sensitive to platform orientation and applied loads than its 3-cable counterpart.

6.4.3 Chord method

The tendon-driven parallel manipulator constant orientation workspaces can also be determined using a modified version of the chord method proposed in Section 5.4. As before the method consists of finding an initial single point on the workspace boundary, and then using an optimization-based search methodology to determine subsequent points along the workspace boundary at constant chord lengths d.

In order to determine a point on the workspace boundary, a single feasible point $\mathbf{u}^0$ somewhere within the workspace boundary must first be determined. This may be accomplished in one of two ways. The first possibility is to run the discretization method, at a coarse resolution to obtain a rough estimation of the workspace. The internal point for the method can then be chosen manually, and the chord methodology used to map the boundary accurately. Alternatively a suitable internal point may be found by solving the following unconstrained optimization problem:

$$\min_{\mathbf{u}} \sum_{i=1}^{n} (t_i - t^{\text{mean}})^2 \tag{6.25}$$

where $t^{\text{mean}} = (t^{\text{max}} - t^{\text{min}})/2$. In the implementation this numerical optimization problem is solved using the efficient Dynamic-Q method developed in Chapter 3.

Once a suitable internal point $\mathbf{u}^0$ has been found, the initial point $\mathbf{b}^1$ on the workspace boundary is found by solution of the following optimization problem which replaces (5.17).

$$\begin{gathered} \max_{r} r^2 \\ \text{such that } t^{\text{min}} \leq t_i(\mathbf{u}(r)) \leq t^{\text{max}} \\ \text{and } l_i(\mathbf{u}(r)) \geq l^{\text{min}} \end{gathered} \tag{6.26}$$

where $\mathbf{u}(r) = \mathbf{u}^0 + r\mathbf{s}^1$ as before and, of course, r is the distance from the internal point $\mathbf{u}^0$. For the 3-cable manipulator, inequality constraint (6.24)

is also included in the optimization problem. The cable tensions $t_i,\ i = 1, 2, \ldots, n$ are calculated using either the constrained ℓ_2-norm or constrained ℓ_1-norm approach with $\mathbf{u} = \mathbf{u}(r)$, and cable lengths $l_i,\ i = 1, 2, \ldots, n$ are given by (6.4).

The chord methodology, with specified chord length d, is embodied in the following optimization problem for the tendon-driven manipulator:

$$\begin{aligned} &\min_{\omega} \omega^2 \\ &\text{such that } t^{\min} \leq t_i(\mathbf{u}) \leq t^{\max} \\ &\text{and } l_i(\mathbf{u}) \geq l^{\min} \end{aligned} \tag{6.27}$$

where, $\mathbf{u} = \mathbf{u}(\omega)$ is given by (5.18). The solution of (6.27) yields the next point $\mathbf{b}^{i+1}$ along the workspace boundary and a vector $\mathbf{s}^{2i} = [s_x^{2i}, s_y^{2i}]^\top$, of magnitude d, pointing from $\mathbf{b}^i$ to $\mathbf{b}^{i+1}$. Once again for the 3-cable manipulator, an additional inequality constraint corresponding to condition (6.24) is also included in the optimization problem. The values of the cable tensions, for any $\mathbf{u}$ and prescribed ϕ^{fix}, are once again calculated using either the constrained ℓ_2-norm or constrained ℓ_1-norm approaches, and the cable lengths using (6.4). The chord method otherwise remains the same as presented in Appendix C.

Choice of optimization method

In previous implementations of the chord method, the numerical optimization algorithms used for solving problems (6.26) and (6.27) were the LfopC method (Snyman [103]), or the more efficient Dynamic-Q method (Chapter 3). These methods performed well in these cases, since the constraints typically appearing in the workspace boundary definition were continuous for the types of parallel manipulators studied. For tendon-driven manipulators, this is not always the case. In particular the constraints corresponding to the cable tension limits (6.21) may be discontinuous on the workspace boundary. Consider Figure 6.6(a) which shows the $\phi_P = 0$ constant orientation

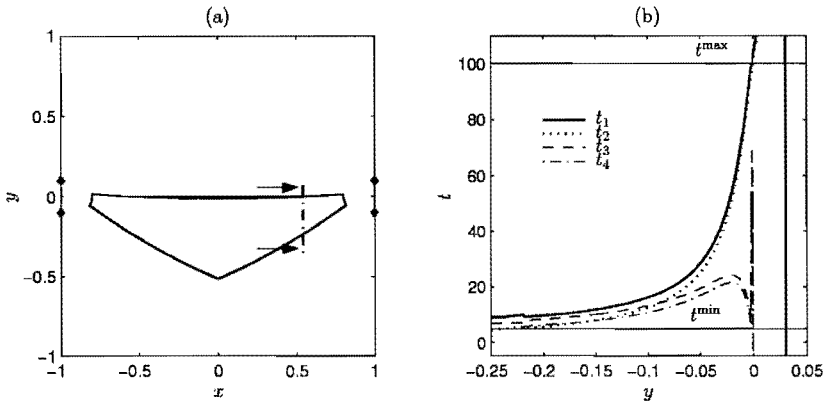

Figure 6.6: (a) Workspace of a 4-cable manipulator with the section indicated by means of the chained line and (b) cable tensions t_i, $i = 1, 2, 3, 4$ along the section

workspace under load case L1 for a 4-cable manipulator with $\mathbf{c}^1 = [1, 0.1]^T$, $\mathbf{c}^2 = [-1, 0.1]^T$, $\mathbf{c}^3 = [-1, -0.1]^T$ and $\mathbf{c}^4 = [1, -0.1]^T$, and platform attachment points $\bar{\mathbf{a}}^i$ as given in Table 6.1. The chained line indicates the position of a section taken though the workspace (at $x = 0.54$), along which the cable tensions have been calculated (Figure 6.6(b)). It is evident from Figure 6.6(b) that cable tensions t_3 and t_4 are discontinuous at $y = 0$, a point which corresponds to the workspace boundary. Clearly, the result of these discontinuities is that it is not possible to use a gradient-based algorithm for solving problems (6.26) and (6.27) at every point on the workspace boundary.

This problem is addressed by using a bisection method to solve problem (6.27). It is possible to use a bisection method here, since there is only one variable, namely ω, to solve for in optimization problem. The exact bisection algorithm used is given in Algorithm 6.3.

It is thus now possible to solve optimization problem (6.27) using the Dynamic-Q optimization method, reverting to the bisection algorithm when the optimization breaks down. On implementation, however, it was found that the bisection algorithm is more economical in solving optimization (6.27) than

Algorithm 6.3 Bisection algorithm

1. Given two successive boundary points $\mathbf{b}^{i-1}$ and $\mathbf{b}^{i}$, with $\mathbf{s}^{2(i-1)} = \mathbf{b}^{i} - \mathbf{b}^{i-1}$, calculate $\mathbf{s}^{1i}$ using equation (C.13). Set $\boldsymbol{\beta} = -\mathbf{s}^{2(i-1)}$, $\mathbf{u}^{\beta} = \mathbf{b}^{i-1}$, $\boldsymbol{\alpha} = d\mathbf{s}^{1i}$ and $\mathbf{u}^{\alpha} = \mathbf{b}^{i} + \boldsymbol{\alpha}$. Choose termination parameter $\varepsilon^{u}(= 10^{-8})$.

2. Set $\boldsymbol{\gamma} = d(\boldsymbol{\alpha} + \boldsymbol{\beta})/(\|\boldsymbol{\alpha} + \boldsymbol{\beta}\|)$. If the sign of the z-component of $\boldsymbol{\alpha} \times \boldsymbol{\beta}$ is negative, then $\boldsymbol{\gamma} = -\boldsymbol{\gamma}$.

3. Determine whether $\mathbf{u}^{\gamma} = \mathbf{b}^{i} + \boldsymbol{\gamma}$ lies within the workspace by evaluating inequalities (6.21) and (6.22) at this point.

4. If $\mathbf{u}^{\gamma}$ is feasible, set $\boldsymbol{\beta} = \boldsymbol{\gamma}$ and $\mathbf{u}^{\beta} = \mathbf{u}^{\gamma}$, else set $\boldsymbol{\alpha} = \boldsymbol{\gamma}$ and $\mathbf{u}^{\alpha} = \mathbf{u}^{\gamma}$.

5. If $\mathbf{u}^{\gamma}$ is feasible, and termination condition $\left\|\mathbf{u}^{\beta} - \mathbf{u}^{\alpha}\right\| \leq \varepsilon^{u}$ is satisfied, set $\mathbf{b}^{i+1} = \mathbf{u}^{\gamma}$, $\mathbf{s}^{2i} = \boldsymbol{\gamma}$ and stop, else go to Step 2.

Dynamic-Q, and is thus used exclusively here in mapping the workspace boundary.

Determining the bifurcation points

As before it is necessary to implement a special procedure for determining bifurcation points separately as they are encountered along the workspace boundary. The reason for this is illustrated in Figure 6.7(a). The dashed line represents the actual workspace boundary, and the solid line the approximation to the workspace obtained using the chord method. Since the chord method maps the workspace boundary at discrete chord lengths d, it is evident that bifurcation points will not be accurately determined, and the approximation to the workspace will be degraded. Thus determining the locations of the bifurcation points is important in order to obtain a more accurate representation of the manipulator workspace.

3-cable manipulator

Figure 6.8 gives various constant orientation workspaces for the 3-cable manipulator computed by the chord method. The workspaces calculated are chosen to correspond to those given in Section 6.4.2, to allow for comparison with the workspaces computed using the discretization method and depicted in Figure 6.4. In calculating these workspaces a chord length of $d = 0.05$ was used, except for the workspaces corresponding to $\phi_P = 0$ with load cases L2 and L3, where a smaller chord length of $d = 0.03$ was used in order to capture all the significant features of the workspace boundary. Similarly in calculating the small left hand part of the workspace for L1 and $\phi_P = 0.05$ a chord length of $d = 0.02$ was used. The average computational time for these workspaces is approximately 0.8s.

It is evident that the workspace representations obtained by means of the chord method are much more accurate and efficient in terms of information stored than those obtained by the discretization method. On the other hand the discretization method does present an extremely robust method for workspace determination, although limited in terms of accuracy and computational efficiency.

4-cable manipulator

The workspaces for the 4-cable manipulator, determined using the chord method with $d = 0.05$ are given in Figure 6.9. A reduced chord length of $d = 0.02$ was used to determine the workspace corresponding to load case L3 and $\phi_P = -0.2$. Average computational time per workspace was 30.12s using the constrained ℓ_2-norm approach for determining cable tensions. It is evident on comparison with the results using the discretization method given in Section 6.4.2 that, for comparable computational effort, the chord method yields a much more accurate representation of the workspace. Once

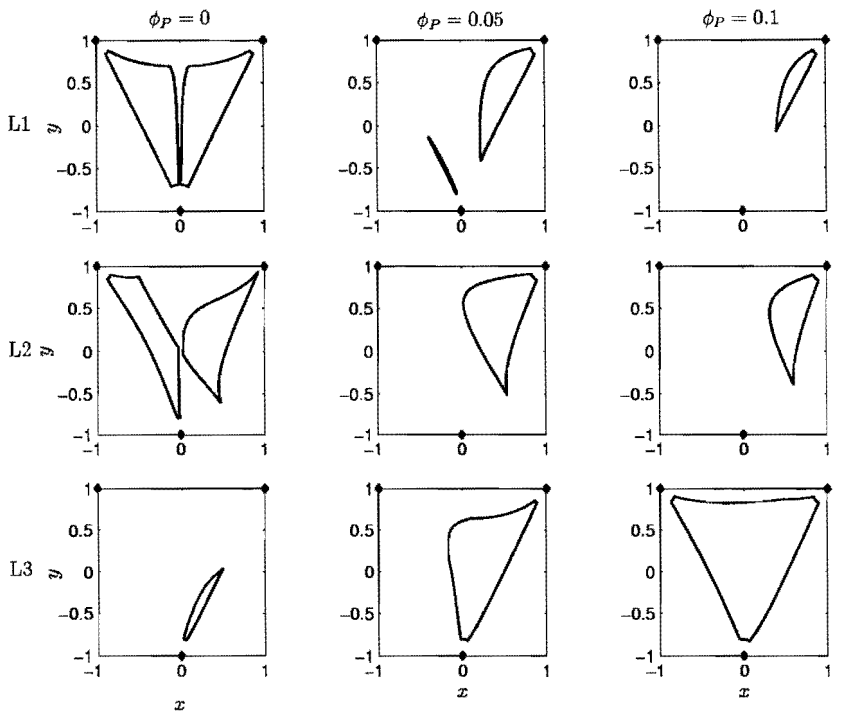

Figure 6.8: Workspaces of the 3-cable TDPM determined using the chord method

again use of the constrained ℓ_1-norm approach for determining the cable tensions results in a much more economical method, with computational times comparable to those of the 3-cable TDPM.

6.5 Dextrous workspace determination

In agreement with the definition given in Section 1.3.1 the dextrous workspace $W^D[\phi^{\min}, \phi^{\max}]$ of the planar tendon-driven manipulator is defined as:

$$\begin{aligned} W^D[\phi^{\min}, \phi^{\max}] = \{ & \mathbf{u} \in \Re^2 : \mathbf{\Phi}(\mathbf{u}, \mathbf{v}, w) = \mathbf{0}; \\ & t^{\min} \leq t_i \leq t^{\max},\ i = 1, 2, \ldots, n; \text{ and} \\ & l_i \geq l^{\min}\ i = 1, 2, \ldots, n \text{ for all } w \in [\phi^{\min}, \phi^{\max}] \} \end{aligned} \tag{6.28}$$

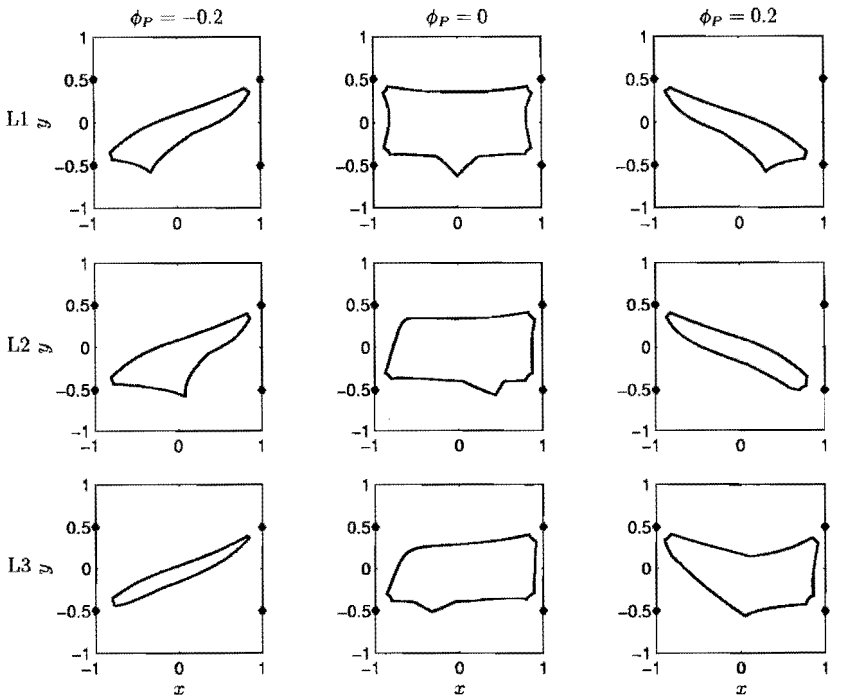

Figure 6.9: Workspaces of the 4-cable TDPM determined using the chord method

The dextrous workspace can be thought of as the intersection of all constant orientation workspaces in the range $[\phi^{\min}, \phi^{\max}]$. Du Plessis and Snyman [18] suggest a numerical approach for determining parallel manipulator dextrous workspaces similar to that used in Section 5.7. Firstly constant orientation workspaces are determined for a finite number m^{sl} of regularly spaced ϕ_P values in the range $[\phi^{\min}, \phi^{\max}]$. The intersection of these constant orientation workspaces then yields the dextrous workspace of the manipulator. In many cases the dextrous workspace may be efficiently and accurately described by simply computing the intersection of the two extreme constant orientation workspaces corresponding to $\phi^{\min}$ and $\phi^{\max}$. Du Plessis and Snyman point out however that it is necessary in this case to also check the validity of this efficient approach by ensuring that the constant orientation workspace at

the intermediate central value of $(\phi^{\min} + \phi^{\max})/2$ fully contains the dextrous workspace computed using the extreme values. In the case where the above-mentioned approach is invalid, the dextrous workspace may be progressively more accurately approximated by increasing m^{sl}, the number of regularly spaced values of ϕ_P between $\phi^{\min}$ and $\phi^{\max}$. The discretization algorithm outlined in the previous section can be easily modified to compute the dextrous workspace, by testing for compliance in Step 4 for a *range* of values of ϕ_P, instead of just one fixed value, as is the case for the constant orientation workspace. This approach is used here instead of that developed in Section 5.5, due to its ease of implementation and slightly higher efficiency.

6.6 Dimensional synthesis for maximal dextrous workspace

6.6.1 Optimization formulation

It is evident from the above results presented in Section 6.4 that the manipulator workspace is highly dependent on the manipulator design, load on the end-effector, and end effector orientation. With this in mind, the problem addressed here is to design the manipulator so that it yields the greatest dextrous workspace for a given load on the platform.

It is assumed that the cable frame attachment points $\mathbf{c}^i$ can be arbitrarily positioned anywhere along the fixed square frame. The angle between the global x-axis and cable attachment point $\mathbf{c}^i$ is denoted β^i. The design vector for the optimization problem is thus $\mathbf{d} = [\beta^1, \beta^2, \ldots, \beta^n]^\top$. The only constraints imposed on the optimization are that a lower limit $\beta^{\min}$ is placed on the angular separations of the frame cable attachment points. The workspace

maximization problem is simply

$$\begin{aligned} &\max_{\mathbf{d}} W^D[\phi^{\min}, \phi^{\max}] \\ \text{such that } &|\beta^{i+1} - \beta^i| \geq \beta^{\min}, \ i = 1, 2, \ldots, n-1 \\ \text{and } &|\beta^n - \beta^1| \geq \beta^{\min} \end{aligned} \tag{6.29}$$

where the necessary adjustments are made to the angular measurements to ensure that the angle determined between consecutive cable attachment points is a minimum.

6.6.2 Numerical results

Optimization formulation (6.29) is used in this section to determine optimum manipulator designs with respect to maximal dextrous workspace for the 3 and 4-cable manipulators. For each manipulator type, optimal manipulator configurations were determined for the three different load cases L1-L3 as given in Table 6.3. It is assumed that these loads are applied at the origin of the moving $x' - y'$ frame. Constrained minimum ℓ_1-norm solutions for cable tensions were used and cable tensions limits were $t^{\min} = 5$ and $t^{\max} = 100$. The optimization problem (6.29) was solved using the Dynamic-Q optimization algorithm (see Chapter 3). As stated previously, this optimization algorithm is suitable for problems where some numerical noise is present in the optimization problem. This is indeed the case here, since the discretization method is used for determining the manipulator dextrous workspaces. Parameters used for the Dynamic-Q method are a move limit of $\rho = 0.1$, a finite difference interval of $\Gamma = 0.05$ for determining the gradients for the 3-cable manipulator, and $\Gamma = 0.1$ for the 4-cable manipulator. Central finite differences were used in calculating these gradients. For the 3-cable manipulator the $[-0.1, 0.1]$ dextrous workspace was computed using a resolution m of 100 points, and m^{sl} of 3. For the 4-cable manipulator, which is capable of reaching a larger workspace, the $[-0.2, 0.2]$ dextrous workspace was computed using a resolution m of 50 points, and m^{sl} of 21. Note that the number

of intermediate values of ϕ_P used for the 3- and 4-cable manipulator differs significantly. This is because just three values of ϕ_P can be used to calculate the 3-cable manipulator dextrous workspaces accurately and efficiently. For the 4-cable manipulator, however, m^{sl} must be increased in order to obtain an accurate description of the dextrous workspace. For both the three and four-cable manipulator and each load case, five feasible random starting designs were chosen for the numerical optimisation embodied in equation (6.29).

3-cable manipulator

Results obtained for the three load cases for 3-cable manipulator are given in Tables 6.5 to 6.7. Each Table gives the number of gradient evaluations N^g of the Dynamic-Q algorithm required to find the solution, the randomly chosen starting design $\mathbf{d}^0$ and area A_d^0 of the associated dextrous workspace, the optimized design $\mathbf{d}^*$ and area A_d^* of the optimized dextrous workspace. Figures 6.10 to 6.12 show results of the dimensional synthesis for representative optimization runs R3, R3 and R1 respectively for load cases L1-L3. In each case Figure (a) shows the starting design and associated workspace, and Figure (b) the optimal design and workspace. Interestingly, for the 3-cable case the dextrous workspace increases in size if a torque is applied to the moving platform. Also of interest when examining the results is the presence of local maxima in the design space. As an example of this see run 4 for L2 (Table 6.6) the solution of which corresponds to a local maxima. The solution obtained by run 4 of L1 (Table 6.5) is the mirror image (about $x = 0$) of the other solutions. The optimization problem thus has two global minima.

4-cable manipulator

Optimization results for the 4-cable manipulator are reported in Tables 6.8 to 6.10. Figures 6.13 to 6.15 once more show representative results from

Run	N^g	$\mathbf{d}^0$	A_d^0	$\mathbf{d}^*$	A_d^*
1	52	$[0.6607, 2.748, 4.367]^\top$	0.0660	$[0.7676, 3.430, 3.605]^\top$	0.3152
2	34	$[0.6725, 2.880, 4.633]^\top$	0.0880	$[0.7631, 3.519, 3.693]^\top$	0.3168
3	39	$[0.2814, 3.978, 4.278]^\top$	0.1996	$[0.7645, 3.477, 3.651]^\top$	0.3172
4	50	$[0.735, 2.418, 5.159]^\top$	0.0024	$[-0.3146, 2.379, 5.794]^\top$	0.3168

Table 6.5: 3-cable TDPM optimized designs for L1

Run	N^g	$\mathbf{d}^0$	A_d^0	$\mathbf{d}^*$	A_d^*
1	17	$[0.9758, 4.056, 4.225]^\top$	0.0216	$[0.6179, 3.703, 3.878]^\top$	0.5136
2	21	$[0.5014, 2.808, 3.616]^\top$	0.0524	$[0.7728, 3.348, 3.523]^\top$	0.5120
3	41	$[0.6861, 2.431, 4.461]^\top$	0.0812	$[0.7667, 3.454, 3.628]^\top$	0.5228
4	55	$[1.864, 2.621, 4.251]^\top$	0.0100	$[1.683, 1.858, 4.389]^\top$	0.2504

Table 6.6: 3-cable TDPM optimized designs for L2

Run	N^g	$\mathbf{d}^0$	A_d^0	$\mathbf{d}^*$	A_d^*
1	83	$[0.7983, 1.281, 3.373]^\top$	0.0500	$[0.6543, 2.357, 4.252]^\top$	1.024
3	5	$[0.6097, 2.319, 4.197]^\top$	0.8364	$[0.6550, 2.371, 4.215]^\top$	1.019
3	48	$[0.3040, 1.220, 5.040]^\top$	0.0028	$[0.6358, 2.366, 4.263]^\top$	1.019
4	45	$[0.5922, 1.718, 4.865]^\top$	0.1736	$[0.6500, 2.369, 4.233]^\top$	1.021

Table 6.7: 3-cable TDPM optimized designs for L3

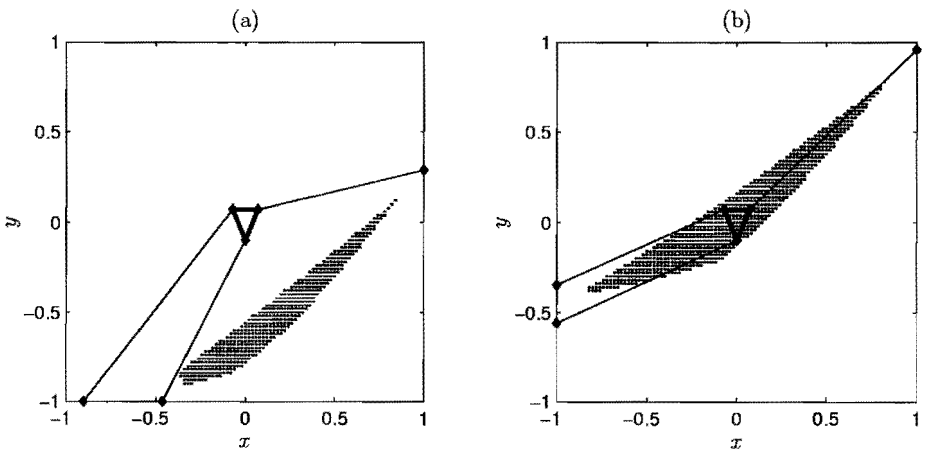

Figure 6.10: 3-cable TDPM (a) starting and (b) optimized design for L1 (R3)

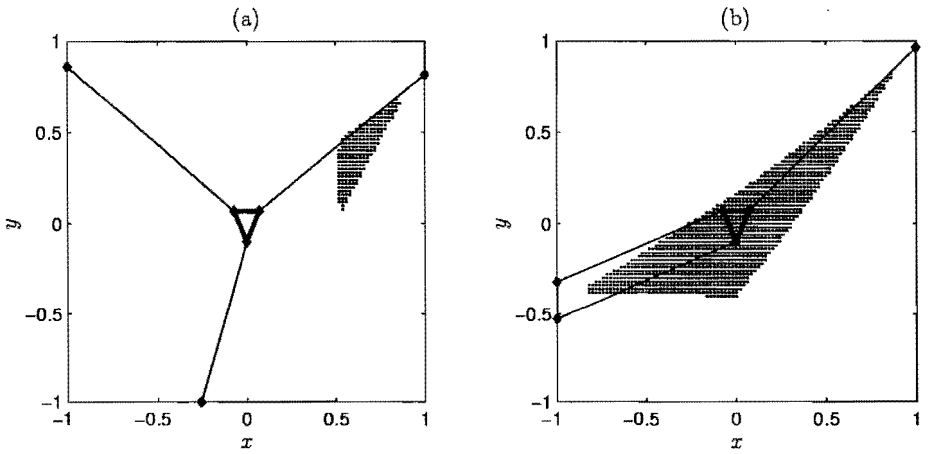

Figure 6.11: 3-cable TDPM (a) starting and (b) optimized design for L2 (R3)

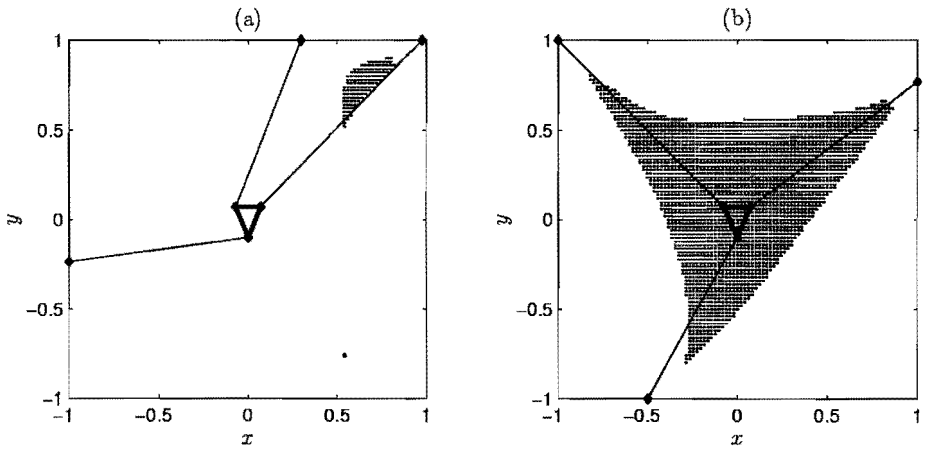

Figure 6.12: 3-cable TDPM (a) starting and (b) optimized design for L3 (R1)

Run	N^g	$\mathbf{d}^0$	A_d^0	$\mathbf{d}^*$	A_d^*
1	48	$[1.829, 2.321, 3.392, 3.741]^\top$	0.0256	$[0.8205, 2.338, 4.595, 4.769]^\top$	1.1040
2	47	$[2.139, 3.124, 3.216, 5.478]^\top$	0.1904	$[0.7878, 3.112, 3.287, 5.582]^\top$	0.9568
3	48	$[2.288, 2.601, 3.876, 4.117]^\top$	0.0144	$[0.8207, 2.335, 4.601, 4.775]^\top$	1.0992
4	14	$[0.7109, 2.219, 4.795, 4.997]^\top$	0.9472	$[0.8123, 2.325, 4.625, 4.799]^\top$	1.0992

Table 6.8: 4-cable TDPM optimized designs for L1

Run	N^g	$\mathbf{d}^0$	A_d^0	$\mathbf{d}^*$	A_d^*
1	34	$[0.0924, 2.607, 2.813, 5.982]^\top$	0.1424	$[0.7403, 3.173, 3.348, 5.564]^\top$	0.9760
2	39	$[1.917, 3.369, 3.745, 3.828]^\top$	0.0272	$[0.8215, 2.334, 4.585, 4.760]^\top$	1.1504
3	56	$[0.4313, 3.742, 4.899, 5.242]^\top$	0.0368	$[0.8194, 2.334, 4.591, 4.765]^\top$	1.1504
4	82	$[0.5235, 2.065, 4.784, 4.913]^\top$	0.5088	$[0.8146, 2.326, 4.609, 4.783]^\top$	1.1472

Table 6.9: 4-cable TDPM optimized designs for L2

the synthesis. For the 4-cable case, local maxima are also found during the design optimization. See for example run 2 for L1, run 1 for L2 and run 3 for L3.

6.7 Conclusion

The new constrained ℓ_2- and ℓ_1-norm approaches for determining cable tensions in overconstrained tendon-driven manipulators are reliable, and indeed critical for the accurate and correct determination of tendon-driven manipulator workspaces. Two methodologies for determining workspaces of planar

Run	N^g	$\mathbf{d}^0$	A_d^0	$\mathbf{d}^*$	A_d^*
1	55	$[1.347, 1.622, 2.036, 5.416]^\top$	0.0048	$[0.7572, 2.922, 3.097, 5.449]^\top$	1.3008
2	17	$[0.4202, 2.962, 3.531, 6.158]^\top$	0.1968	$[0.7636, 2.929, 3.104, 5.439]^\top$	1.2944
3	37	$[0.6810, 0.9393, 3.676, 5.416]^\top$	0.0016	$[1.452, 1.626, 3.843, 5.406]^\top$	0.8304
4	23	$[0.1010, 2.683, 4.338, 4.407]^\top$	0.2032	$[0.8095, 2.330, 4.444, 4.619]^\top$	1.1920

Table 6.10: 4-cable TDPM optimized designs for L3

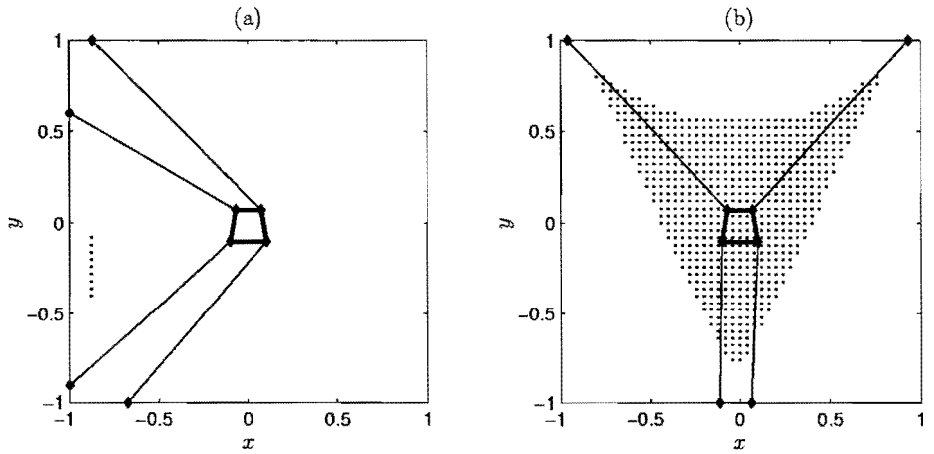

Figure 6.13: 4-cable TDPM (a) starting and (b) optimized design for L1 (R3)

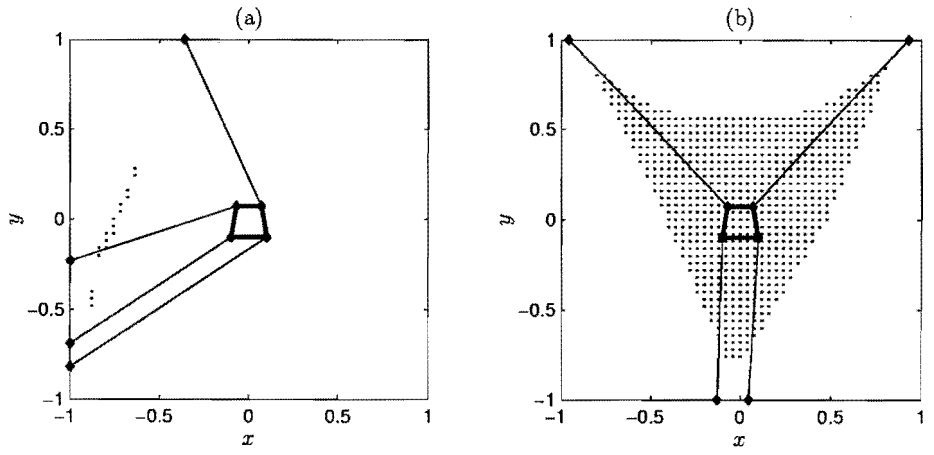

Figure 6.14: 4-cable TDPM (a) starting and (b) optimized design for L2 (R2)

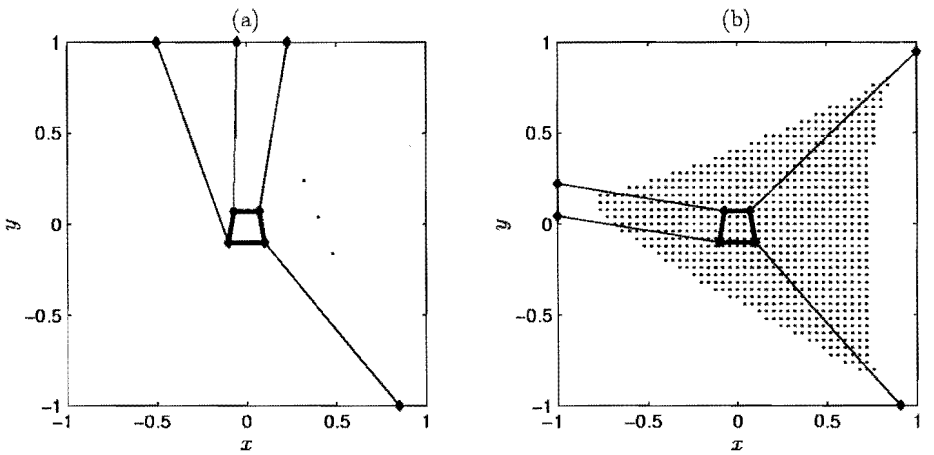

Figure 6.15: 4-cable TDPM (a) starting and (b) optimized design for L3 (R1)

tendon-driven manipulators are presented and evaluated by application to the 3-cable and 4-cable tendon-driven parallel manipulators. The discretization method is robust and reliable, but has a high computational requirement in comparison to the accuracy of the workspace determination. The chord method is accurate, reliable and efficient, but may require some user interaction in selecting the initial point for starting the workspace computation. In practice a combination of the two methods proves to be the most reliable and accurate, first using the discretization method at a low resolution to obtain a rough estimate of the workspace, and then reverting to the chord method to obtain an accurate and efficient mapping of the workspace boundary.

The dimensional synthesis yields TDPM designs with maximal dextrous workspaces for given static loads on the platform. The high dependance of TDPM workspaces on their design is illustrated, demonstrating the importance of dimensional synthesis of such manipulators.